Self-Assembly of Platinum(II) 6-Phenyl-2,2'-Bipyridine Complexes with Solvato- and Iono-Chromic Phenomena

*Jiangjun Chen, Lei Ao, Chengpeng Wei, Cong Wang, and Feng Wang**

CAS Key Laboratory of Soft Matter Chemistry, iChEM,
Department of Polymer Science and Engineering,
University of Science and Technology of China,
Hefei, Anhui 230026 (P. R. China)
Fax: (+86) 551 6360 6095; E-mail: drfwang@ustc.edu.cn.

Supporting Information

1.	*Materials and Methods*	S2
2.	*Self-assembly behaviors of* ***1a–b***	S4
3.	*Self-assembly behaviors of* ***2***	S7
4.	*Synthetic routes to monomers* ***1a–b*** *and* ***2***	S10

1. Materials and Methods

All reagents were employed as purchased. Chloro(6-phenyl-2,2'-bipyridine) platinum **4**,[S1] chloro[2-(4,4'-di-*tert*-butyl-2,2'-bipyridin-6-yl)phenyl] platinum **5**,[S2] 1,2,3-tris(dodecyloxy)-5-isocyanobenzene,[S3] compounds **6**,[S4] and **3**[S5] were synthesized according to the previously reported procedures.

^{1}H NMR spectra were collected on a Varian Unity INOVA-300 spectrometer with TMS as the internal standard. ^{13}C NMR spectra were recorded on a Varian Unity INOVA-300 spectrometer at 75 MHz. Electrospray ionization mass spectra (ESI-MS) were obtained on a Bruker Esquire 3000 plus mass spectrometer (Bruker-Franzen Analytik GmbH Breman, Germany) equipped with an ESI interface and ion trap analyzer. UV/Vis spectra were recorded on UV-1800 Shimadzu spectrometer. Steady-state emission spectra were recorded on a FluoroMax-4 spectrofluorometer (Horiba Scientific), and analyzed with an Origin (*v*8.1) integrated software FluoroEssence (*v*2.2).

To acquire the detailed thermodynamic parameters for the temperature-dependent self-assembly process, the obtained UV–Vis spectra date is normalized between 0 and 1 using the following **Eq. S1**. The normalized UV–Vis heating curve is further fitted by the Meijer−Smulders mathematical model,[S6] which is depicted by **Equation. S2**.

$$\alpha_{agg}(T) = \frac{A(T) - A_{mom}}{A_{agg} - A_{mom}} \qquad \textbf{(Eq. S1)}$$

$$\alpha_{agg}(T) = \frac{1}{1+\exp[\frac{T-T_m}{T^*}]} \qquad \textbf{(Eq. S2)}$$

In these equations, $A_{(T)}$ is UV–Vis spectra absorbance date at a given temperature. $A_{(mom)}$ is the UV–Vis absorbance date at high temperature or good solvent corresponding to the monomer state, while $A_{(agg)}$ is UV–Vis spectra absorbance date at a given low temperature or poor solvent corresponding to the fully aggregated state. The obtained fraction of aggregates (α) *versus* temperature (K) was fitted to the temperature-dependent isodesmic model by Origin (*v*8.1). In the **Eq. S2**, T_m is the melting temperature or temperature at which the fraction of aggregates (α_{agg}) is 0.5; T^* value is obtained by fitting equation (**Eq. S2**) to the experimental data.

For the solvent-dependent UV–Vis measurements, a sigmoidal denaturation curve is obtained upon plotting α_{agg} *vs* the TCE volume fraction (*f*). The curve can be further fitted by an earlier reported equilibrium model adapted to solvent-dependent association using Matlab,[S7] In this equilibrium model, the assembly process is described as a sequence of monomer addition equilibria with equilibrium constant K_e. In the case of cooperative growth, the monomer addition steps in the nucleation regime (up to nucleus size *n*) are described by equilibrium

constant K_n, with cooperativity parameter $\sigma = K_n/K_e < 1$ [Obviously, in an isodesmic supramolecular polymerization, $K_n = K_e$ ($\sigma = 1$)]. The equilibrium constant K_e is defined *via* $K_e = \exp(-\Delta G_f/RT)$, with ΔG_f being the Gibbs free energy gain upon monomer addition, R the gas constant, and T the temperature. In an analogy with protein denaturation models, the Gibbs free energy is assumed to be linearly dependent on the volume fraction of TCE which is described by **Eq. S3**:

$$\Delta G_f = \Delta G_0 + m \times f \qquad \textbf{(Eq. S3)}$$

In this equation, ΔG_f is the Gibbs free energy of monomer association on the TCE volume fraction f, ΔG_0 represents the Gibbs free energy gain upon monomer association in pure MCH. The dependence of ΔG_f on f is described by the m-value.

*2. Self-assembly behaviors of **1a–b***

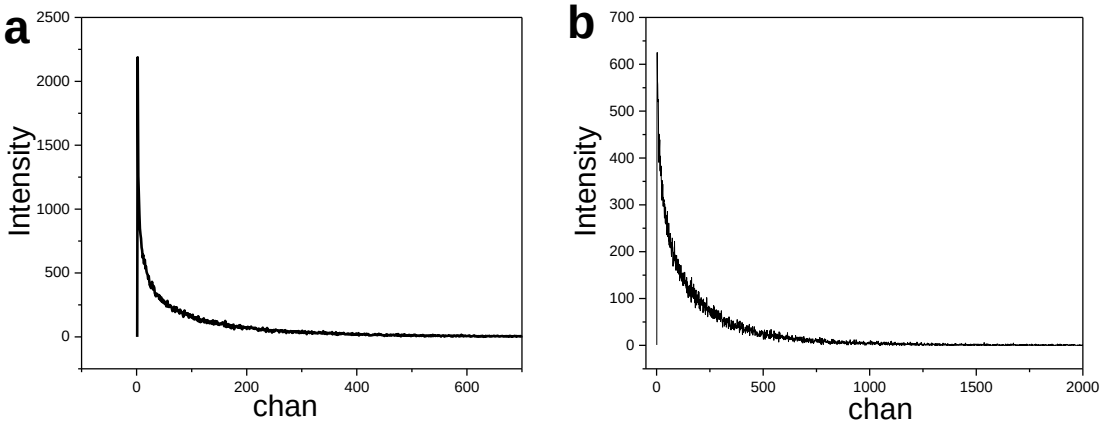

Figure S1. Emission lifetime measurements for (a) **1a** in MCH/TCE (80 : 20, *v*/*v*, 1.0 × 10^{-4} M), and (b) **1b** in MCH (1.0 × 10^{-4} M). The lifetimes are determined to be 0.48 μs and 0.66 μs for **1a** and **1b**, respectively, denoting the involvement of triplet emission character for both systems.

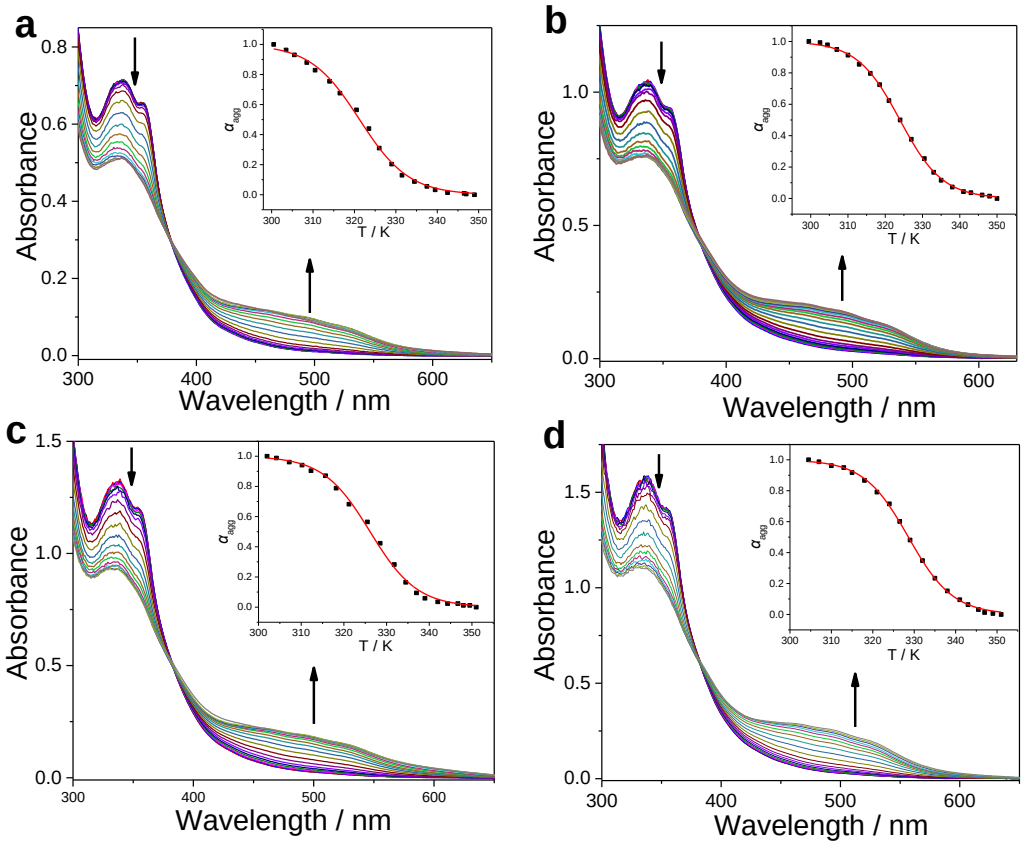

Figure S2. Temperature-dependent UV–Vis absorption spectra of **1a** at the different monomer concentrations: (a) 7.50 × 10^{-5} M; (b) 1.00 × 10^{-4} M; (c) 1.25 × 10^{-4} M; (d) 1.50 × 10^{-4} M in MCH/TCE (80 : 20, *v*/*v*, 10 mm cuvette). The arrows indicate the spectral changes upon decreasing the temperature. Inset: degree of aggregation α_{agg} as a function of temperature. The red lines denote the mathematical model fitting of the curves.

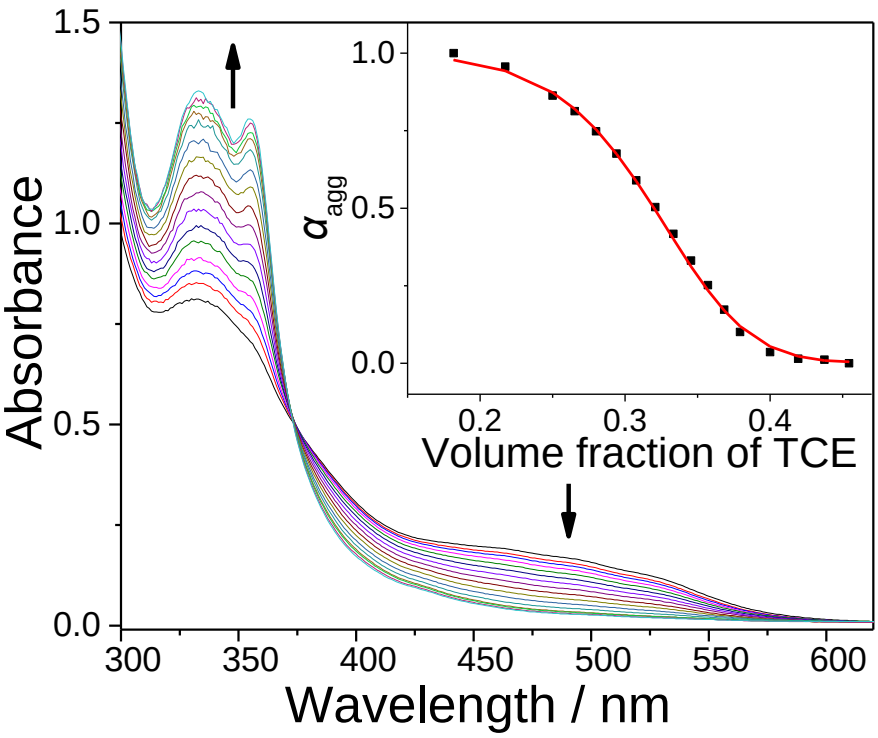

Figure S3. Solvent-dependent UV–Vis absorption spectra of **1a** (1.0×10^{-4} M in MCH/TCE (80 : 20, *v*/*v*, 10 mm cuvette). The arrow indicates the spectral changes upon increasing the TCE fraction. Inset: degree of aggregation α_{agg} as a function of TCE volume fraction monitored at 500 nm. The red line denotes the mathematical model fitting of the curve according to a solvent-dependent equilibrium model. The self-assembly process conforms to the isodesmic mechanism, in which the ΔG_0 (Gibbs free energy gain upon monomer association in pure MCH), *m* and cooperativity parameter (σ) values are determined to be –47 kJ mol^{-1}, 71.5 kJ mol^{-1} and 1, respectively. According to Eq. S3, ΔG value is determined to be –32.7 kJ·mol^{-1} in MCH/TCE (80 : 20, *v*/*v*).

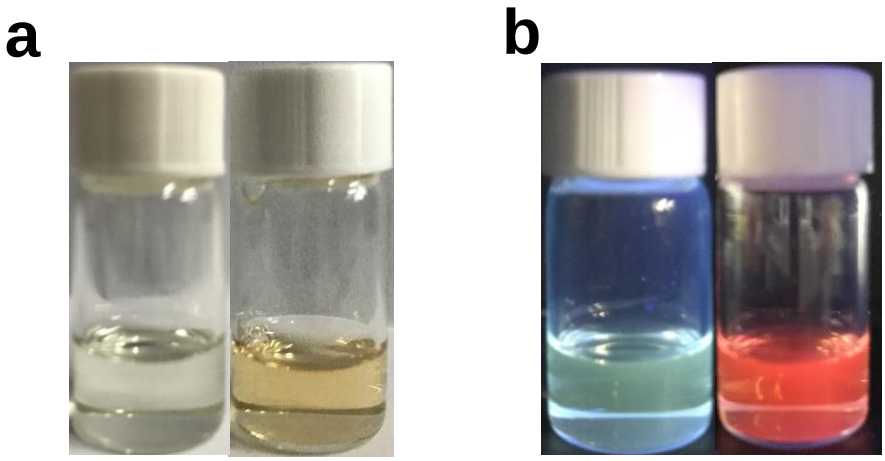

Figure S4. Chromic phenomena for monomer **1b**, as reflected by the color/luminescence difference in MCH/TCE (90 : 10, *v*/*v*) (left) and MCH (right): (a) under the sunlight; (b) under the 365 nm UV lamp.

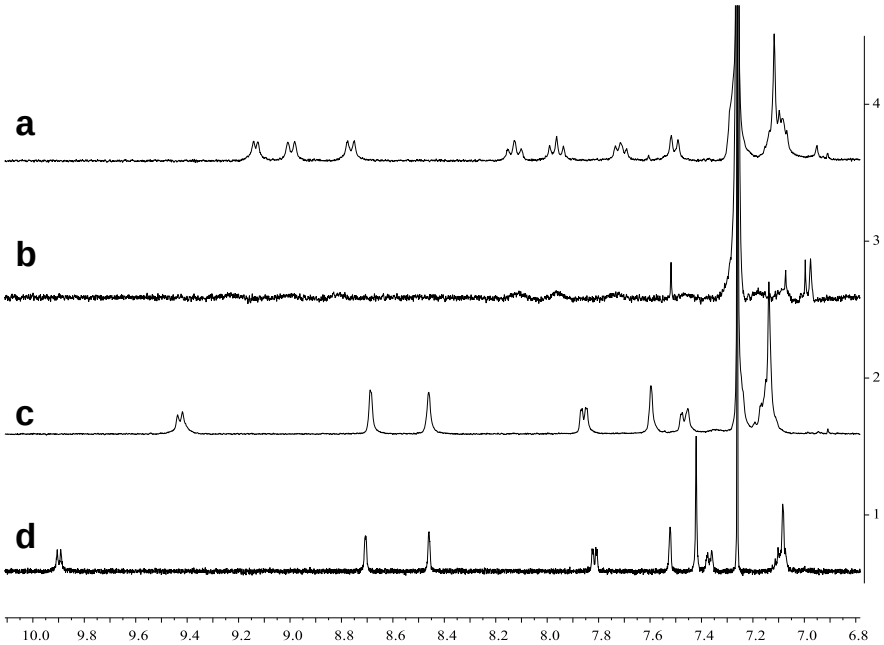

Figure S5. ^{1}H NMR spectra (300 MHz, 298 K, 3.00 mM) of (a) **1a** in $CDCl_3$, (b) **1a** in MCH/$CDCl_3$ (40 : 60, *v*/*v*), (c) **1b** in $CDCl_3$, and (d) **1b** in MCH/$CDCl_3$ (40 : 60, *v*/*v*). Monomer **1b** shows sharp aromatic resonances in both $CDCl_3$ and MCH/$CDCl_3$ (60 : 40, *v*/*v*), denoting the dominance of monomeric state. In terms of **1a**, well-defined signals can be observed in $CDCl_3$. In sharp contrast, broad and bad-resolved signals are observed in MCH/$CDCl_3$ (60 : 40, *v*/*v*), suggesting the formation of oligomeric assemblies for **1a** in the latter solvent medium. By comparing the ^{1}H NMR signals of **1a** and **1b** in the apolar medium, it is apparent that the steric hindrance groups on **1b** weaken intermolecular π–π stacking interactions, which further influence the stability and gelation capability of supramolecular assemblies.

*3. Self-assembly behaviors of **2***

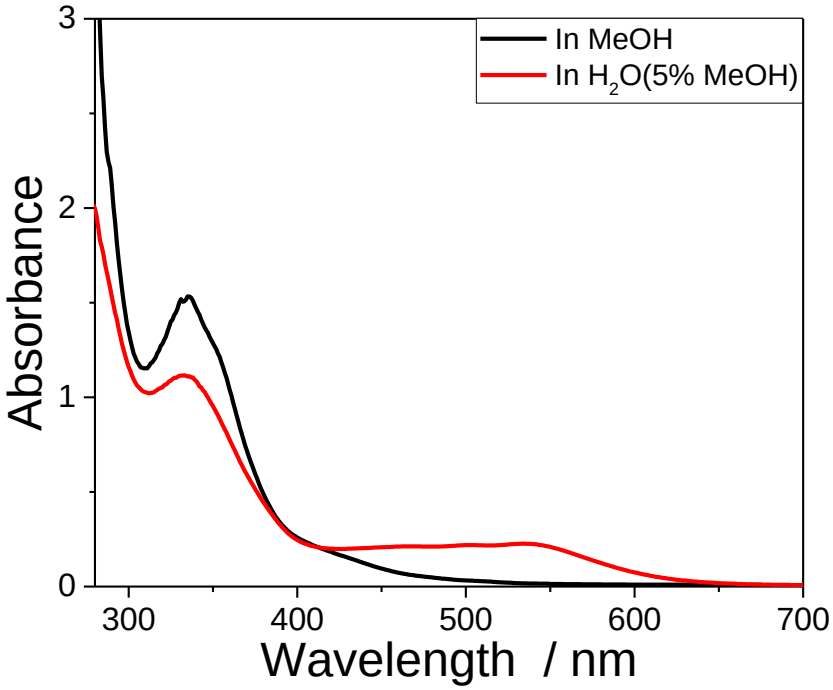

Figure S6. UV–Vis spectra of **2** (5.00×10^{-5} M) in MeOH (black line) and in water/MeOH (95 : 5, *v*/*v*; red line). π–Stacking and Pt···Pt metal–metal interactions tend to form in water/MeOH (95 : 5, *v*/*v*), as evidenced by the appearance of MMLCT absorbance centered at 535 nm.

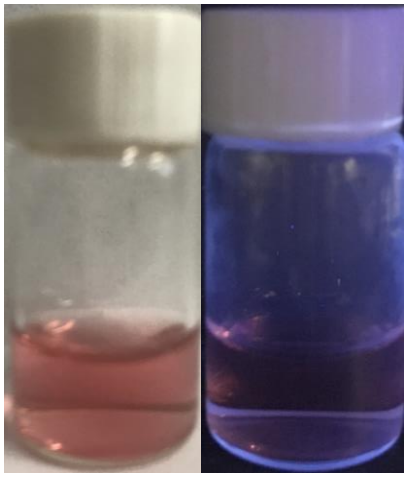

Figure S7. Monomer **2** in water/MeOH (95 : 5, *v*/*v*) under the sunlight (*left*) and 365 nm UV lamp (*right*). The absence of emission signals is primarily ascribed to the existence of tetra(oxyethylene) spacer on **2**, which quenches luminescence *via* photo-induced electron transfer process.

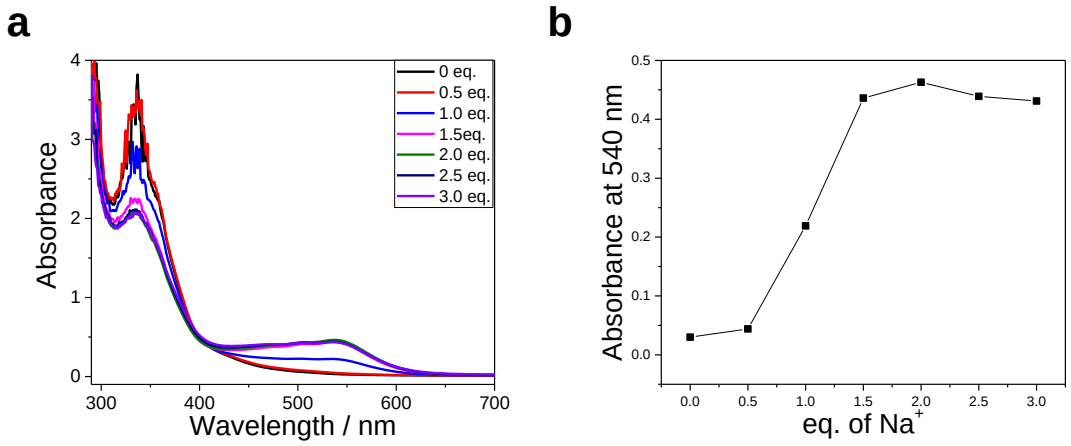

Figure S8. (a) UV–Vis spectra of **2** (1.00 × 10^{-4} M) with the different equivalent amount of $NaClO_4$ in $CHCl_3$/MeOH (50 : 50, *v*/*v*). (b) Absorbance intensity at 540 nm *versus* the amount of $NaClO_4$.

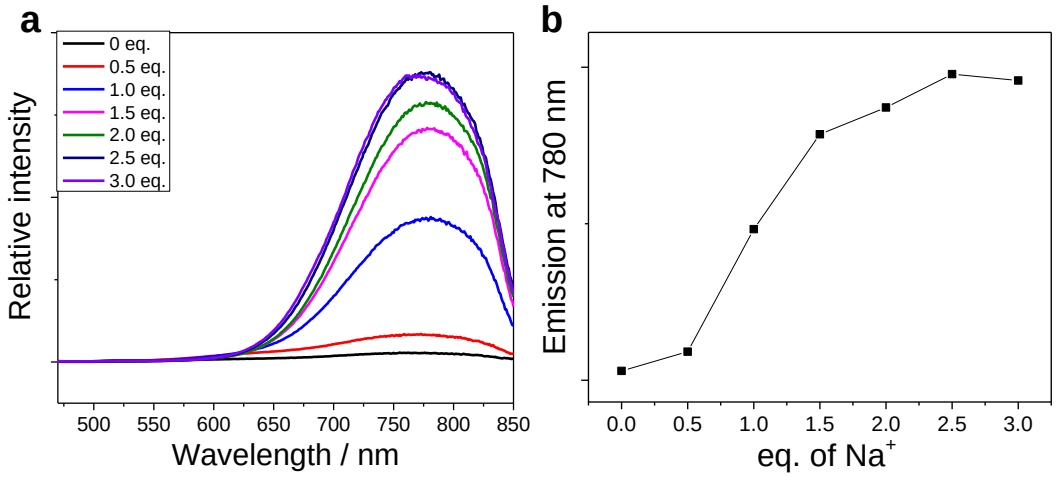

Figure S9. (a) Normalized emission spectra of **2** (1.00 × 10^{-4} M, λ_{ex} = 450 nm) with the different equivalent amount of $NaClO_4$ in $CHCl_3$/MeOH (50 : 50, *v*/*v*). (b) Emission intensity at 780 nm *versus* the amount of $NaClO_4$.

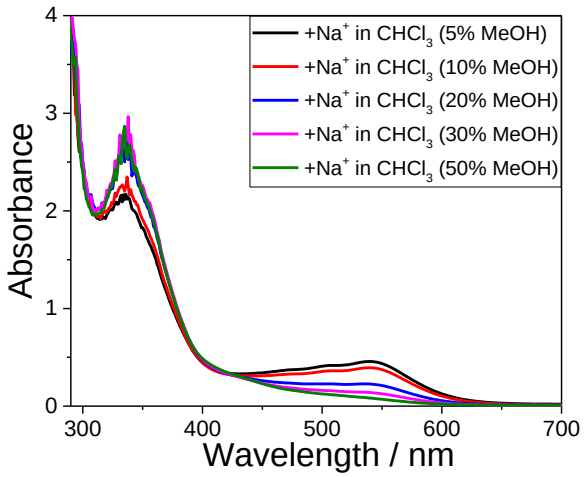

Figure S10. Solvent-dependent UV–Vis spectra for a 1 : 1.5 mixture of **2** (1.00 × 10^{-4} M) and $NaClO_4$ in $CHCl_3$/MeOH media. Upon increasing MeOH fraction in the mixed solvent,

MMLCT bands significantly decrease for their intensities, and totally disappear at the $CHCl_3$/MeOH volume ratios of 50 : 50 (*v*/*v*). It is rationalized that Na^+ cation could probably be entrapped by the methanol solvent, which reduce the opportunity for Na^+–tetra(oxyethylene) complexation.

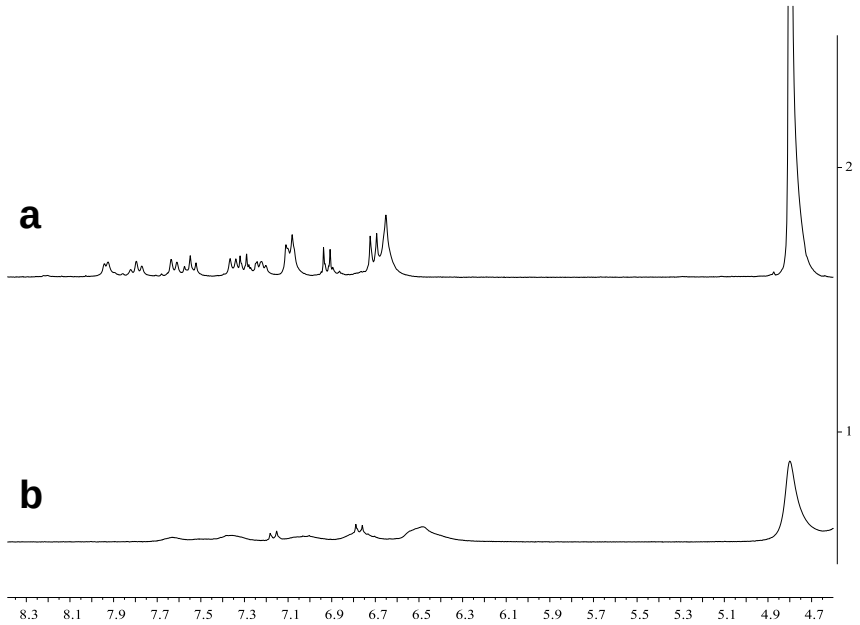

Figure S11. ^{1}H NMR spectra (300 MHz, 298 K, 3.00 mM) of **2**: (a) in CD_3OD, (b) in D_2O/CD_3OD (40 : 60, *v*/*v*). Well-defined signals can be observed in CD_3OD, denoting the dominance of monomeric state. In comparison, broad and bad-resolved signals are observed in D_2O/CD_3OD (40 : 60, *v*/*v*), suggesting the formation of oligomeric face-to-face stacks.

*4. Synthetic routes to monomers **1a**–**b** and **2***

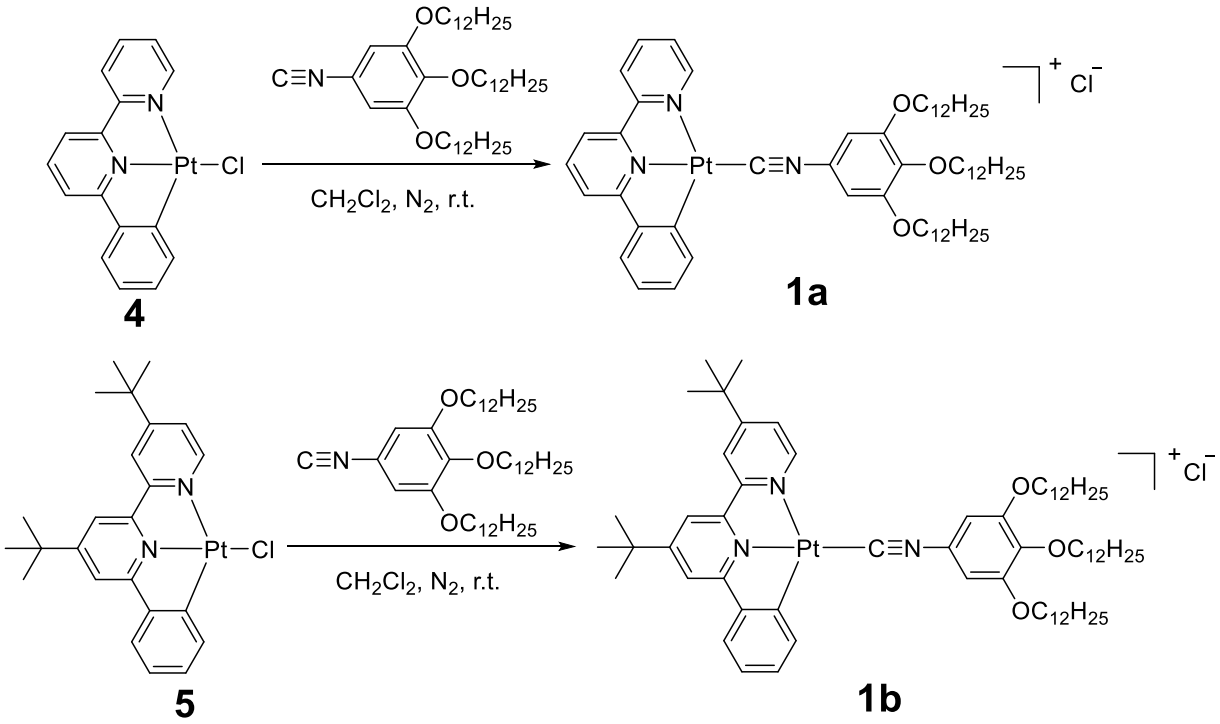

Scheme S1. Synthetic route to the designed monomers **1a**–**b**.

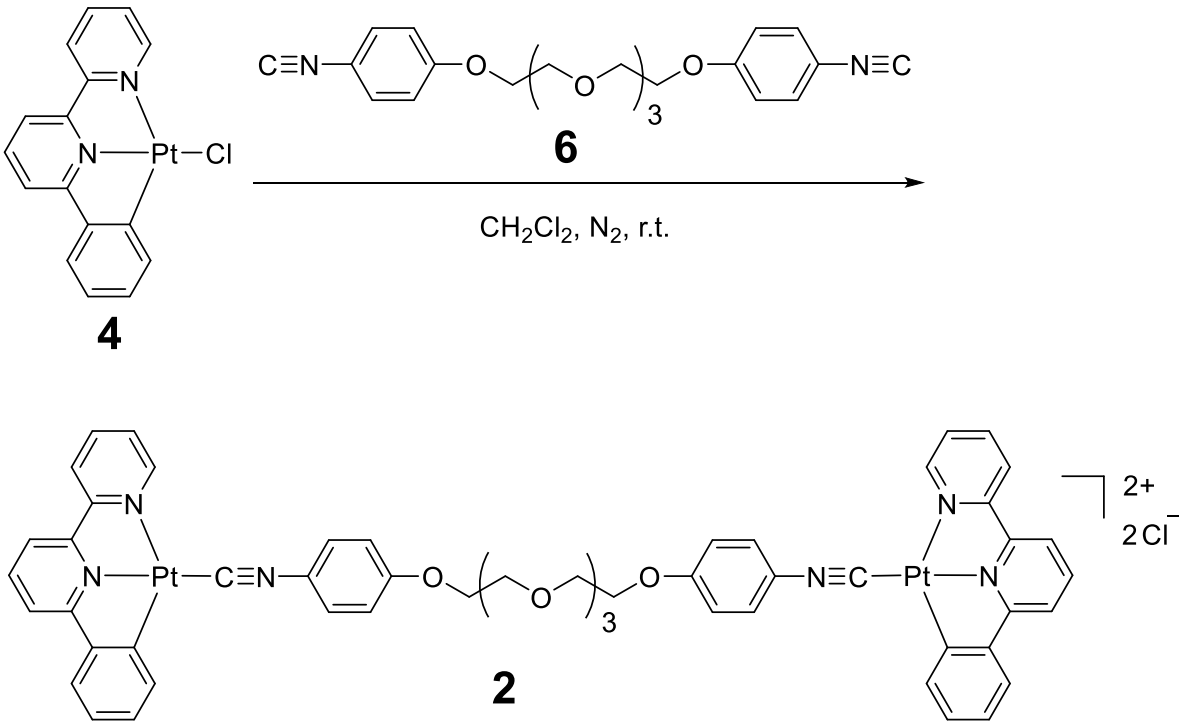

Scheme S2. Synthetic route to the designed monomer **2**.

4.1. Synthesis of ***1a***

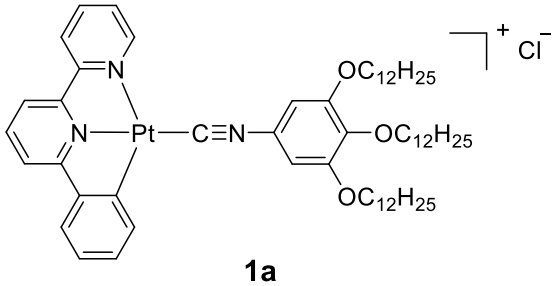

1a

Compound **4** (200 mg, 0.43 mmol), 1,2,3-tris(dodecyloxy)-5-isocyanobenzene (284 mg, 0.43 mmol) were mixed together in CH_2Cl_2 (50 mL), and stirred at room temperature for 12 hours. The reaction mixture was then evaporated, and recrystallized by the diffusion of diethyl ether vapor into the dichloromethane solution of **1a**. The targeted compound was obtained as a yellow solid (400 mg, yield: 83%). ^{1}H NMR (300 MHz, $CDCl_3$) δ (ppm): 9.14 (s, 1H), 8.71 (s, 1H), 8.38 (s, 1H), 7.88 (s, 1H), 7.61 (s, 2H), 7.33 (s, 1H), 7.09 (s, 3H), 6.98–6.78 (m, 3H), 4.11 (s, 4H), 4.00 (t, J = 6.3 Hz, 2H), 2.01–1.45 (m, 12H), 1.43–1.13 (m, 48H), 0.88 (t, J = 6.3 Hz, 9H). ^{13}C NMR [75 MHz, $CDCl_3/CD_3OD$ (9 : 1, v/v)] δ (ppm): 163.8, 155.5, 153.8, 152.7, 152.2, 145.6, 142.5, 140.8, 139.8, 136.6, 136.0, 131.3, 130.1, 128.5, 125.5, 124.3, 119.3, 104.3, 73.0, 68.9, 31.0, 29.4, 28.8, 28.7, 28.4, 25.2, 21.7, 13.1. MALDI−TOF−MS m/z: $[M - Cl]^+$ $C_{59}H_{88}N_3O_3Pt^+$, 1081.6355.

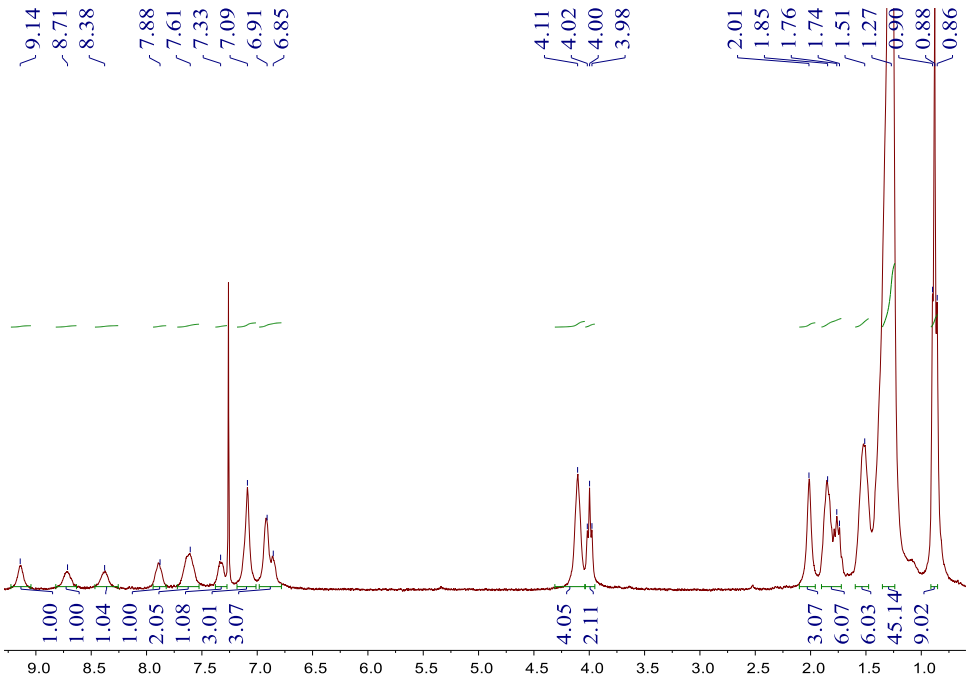

Figure S12. ^{1}H NMR spectrum (300 MHz, $CDCl_3$, 298 K) of **1a**.

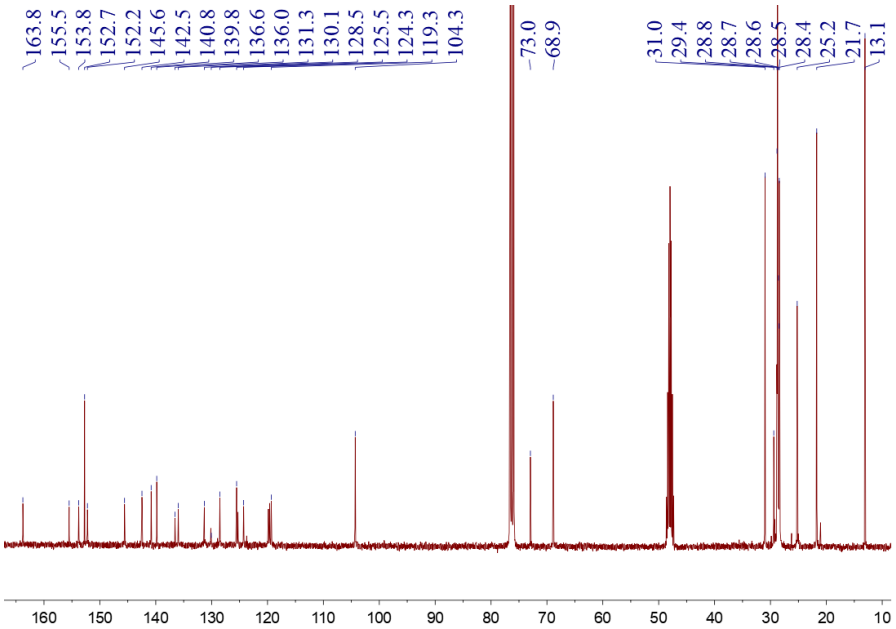

Figure S13. ^{13}C NMR spectrum (75 MHz, $CDCl_3/CD_3OD$ (9 : 1, *v*/*v*), 298 K) of **1a**.

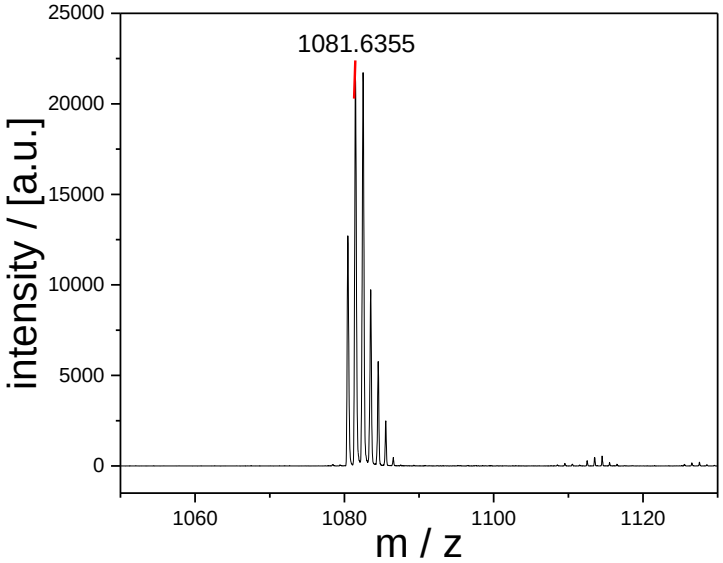

Figure S14. MALDI−TOF−MS spectrum of **1a**.

*4.2. Synthesis of **1b***

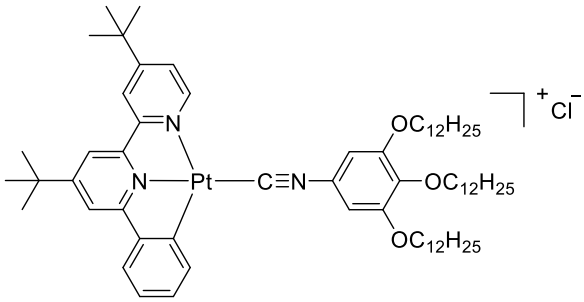

1b

Compound **5** (200 mg, 0.35 mmol), 1,2,3-tris(dodecyloxy)-5-isocyanobenzene (229 mg, 0.35 mmol) were mixed together in CH_2Cl_2 (50 mL), and stirred at room temperature for 12 hours. The reaction mixture was then evaporated, and recrystallized by the diffusion of diethyl ether vapor into the dichloromethane solution. The targeted compound **1b** was obtained as a yellow solid (364 mg, yield: 85%). ^{1}H NMR (300 MHz, $CDCl_3$) δ (ppm): 9.56 (d, J = 5.7 Hz, 1H), 8.66 (s, 1H), 8.41 (s, 1H), 7.82 (dd, J = 5.7, 2.0 Hz, 1H), 7.55 (d, J = 1.3 Hz, 1H), 7.42 (d, J = 6.6 Hz, 1H), 7.20 (s, 2H), 7.16–7.08 (m, 3H), 4.12 (t, J = 6.3 Hz, 4H), 4.00 (t, J = 6.5 Hz, 2H), 1.88–1.81 (m, 4H), 1.79–1.72 (m, 2H), 1.69 (s, 6H), 1.54 (s, 9H), 1.43 (s, 9H),1.37–1.23 (m, 48H), 0.89–0.85 (m, 9H). ^{13}C NMR (75 MHz, $CDCl_3$) δ (ppm): 167.1, 165.1, 162.8, 155.5, 154.4, 154.2, 152.6, 145.8, 139.5, 137.6, 135.4, 130.7, 125.0, 124.8, 124.2, 121.4, 120.4, 117.0, 115.1, 105.1, 72.7, 69.1, 35.7, 35.1, 30.9, 29.6, 29.2, 28.7, 28.5, 25.1, 21.7, 13.1. MALDI−TOF−MS m/z: $[M - Cl]^+$ $C_{67}H_{104}N_3O_3Pt^+$, 1193.7845.

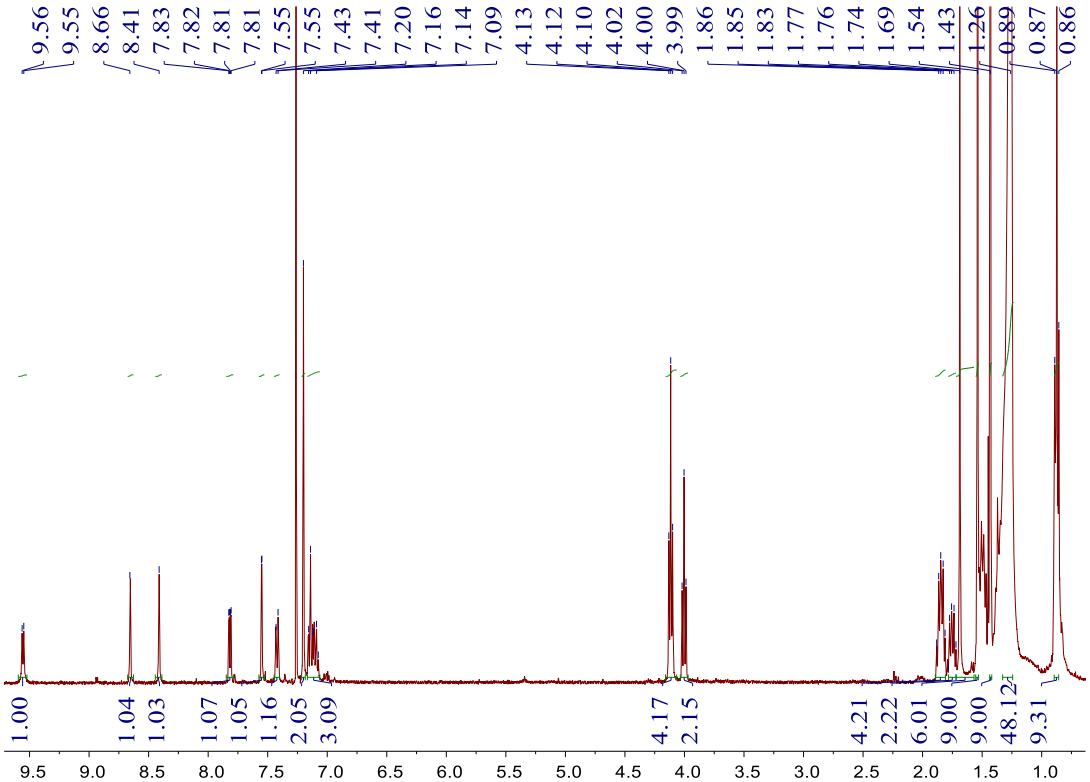

Figure S15. ^{1}H NMR spectrum (300 MHz, $CDCl_3$, 298 K) of **1b**.

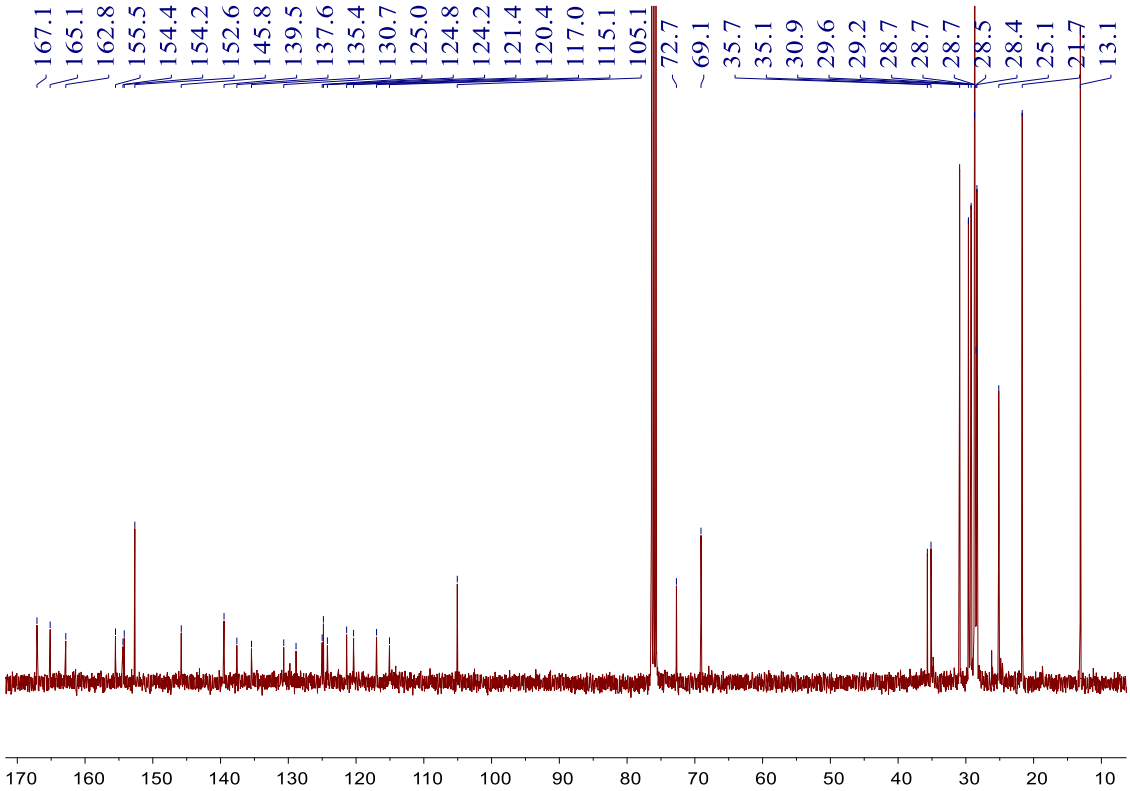

Figure S16. ^{13}C NMR spectrum (75 MHz, $CDCl_3$, 298 K) of **1b**.

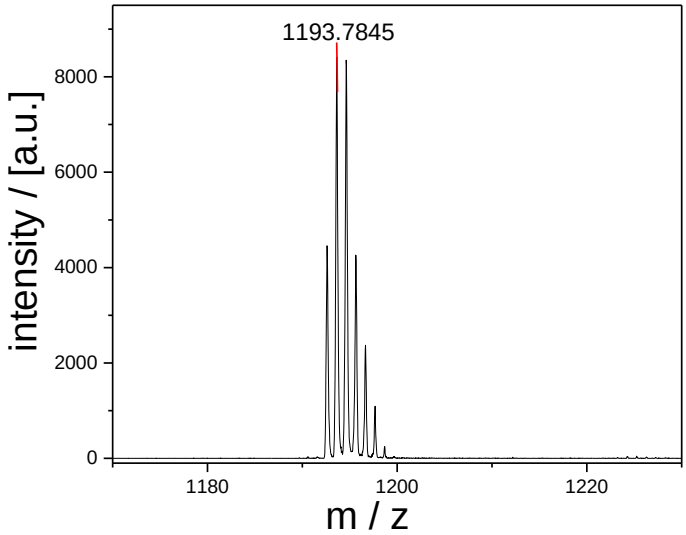

Figure S17. MALDI−TOF−MS spectrum of **1b**.

*4.3. Synthesis of **2***

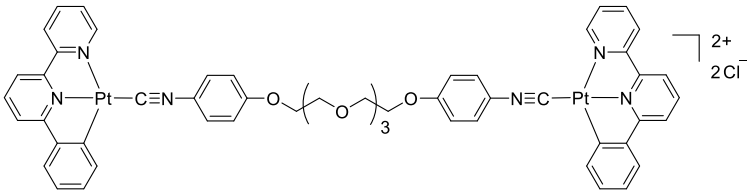

2

Compounds **4** (200 mg, 0.43 mmol), **5** (86.0 mg, 0.22 mmol) were mixed together in CH_2Cl_2 (50 mL), and stirred at room temperature for 12 hours. The reaction mixture was then evaporated, and recrystallized by the diffusion of diethyl ether vapor into the dichloromethane solution. The targeted compound **2** was obtained as a yellow solid (247 mg, yield: 87%). ^{1}H NMR (300 MHz, CD_3OD) δ (ppm): 7.85 (s, 2H), 7.78–7.70 (m, 2H), 7.56 (d, J = 8.7 Hz, 2H), 7.52–7.45 (m, 2H), 7.29(d, J = 7.4 Hz, 2H), 7.21–7.14 (m, 2H), 7.03 (t, J = 8.8 Hz, 6H), 6.68 (d, J = 8.5 Hz, 4H), 6.59 (s, 8H), 4.03 (m, 4H), 3.90 (m, 4H), 3.72 (m, 8H). ^{13}C NMR [75 MHz, $CDCl_3/CD_3OD$ (1 : 1, v/v)] δ (ppm): 163.9, 161.0, 155.7, 154.2, 152.8, 145.8, 143.0, 141.1, 138.7, 136.4, 132.7, 131.0, 130.2, 129.8, 128.7, 126.6, 125.0, 120.4, 118.2, 116.1, 71.0, 69.8, 68.7, 36.0, 32.3, 30.1, 29.7, 26.2, 23.0, 14.1. MALDI−TOF−MS m/z: $[M - 2Cl]^{2+}$ $C_{54}H_{46}N_6O_5Pt_2^{2+}$, 624.1378.

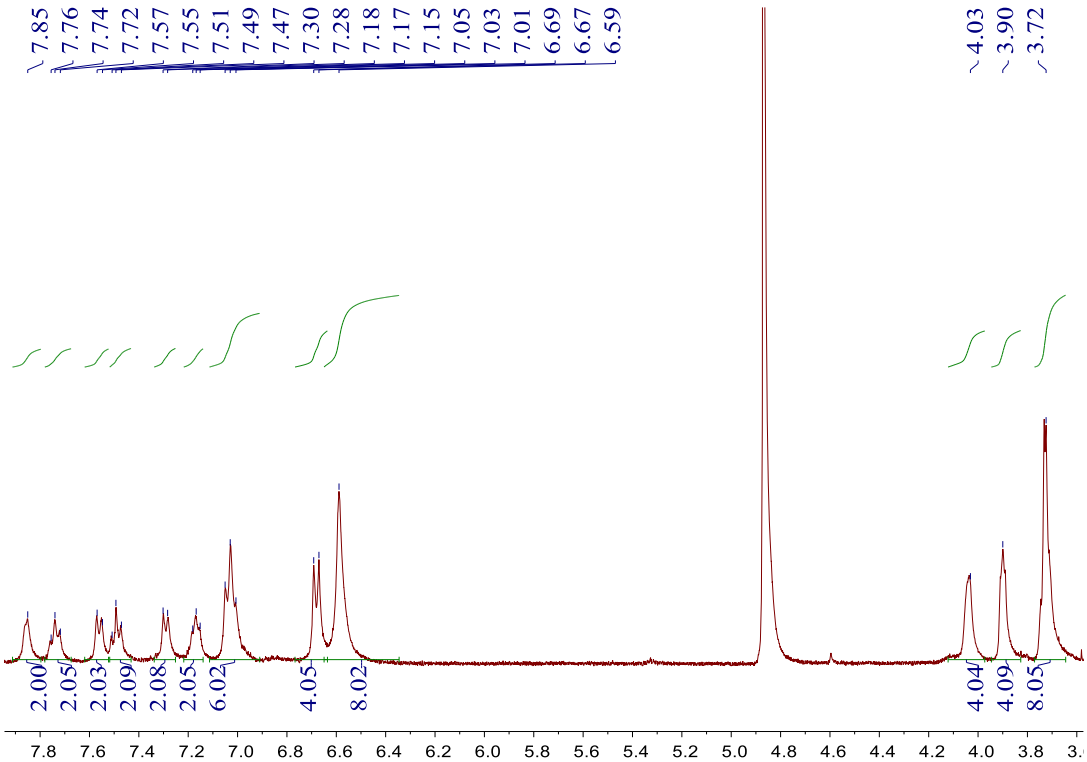

Figure S18. ^{1}H NMR spectrum (300 MHz, CD_3OD, 298 K) of **2**.

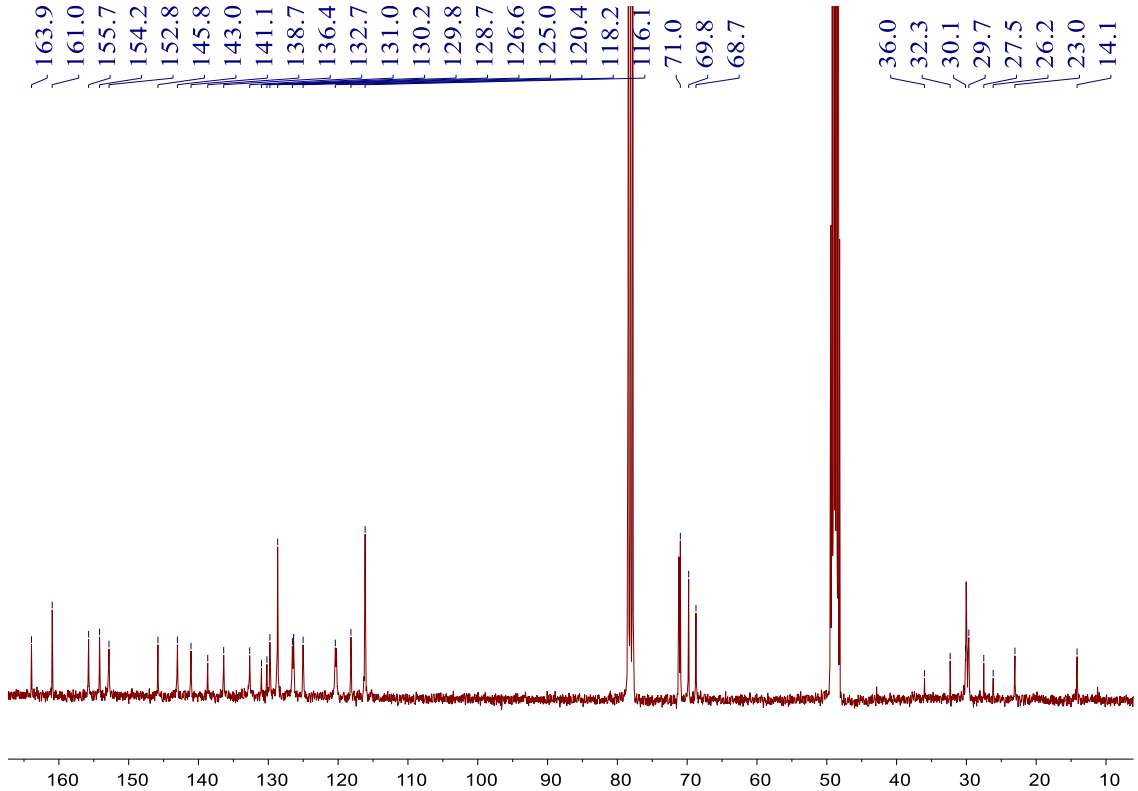

Figure S19. ^{13}C NMR spectrum (75 MHz, $CDCl_3/CD_3OD$ (1 : 1, *v*/*v*), 298 K) of **2**.

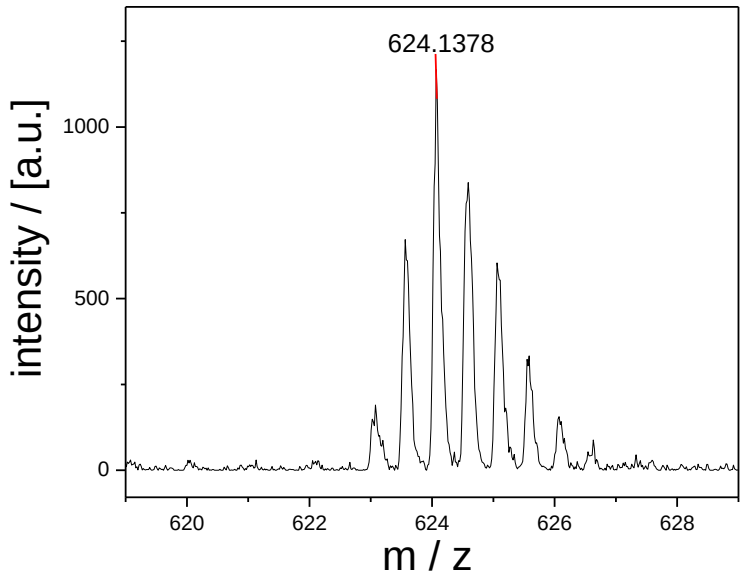

Figure S20. MALDI−TOF−MS spectrum of **2**.

References:

[S1] W. Lu, Y. Chen, V. A. L. Roy, S. S.-Y. Chui, and C.-M. Che, *Angew. Chem. Int. Ed.*, 2009, **48**, 7621.

[S2] P. Savel, C. Latouche, T. Roisnel, H. Akdas-Kilig, A. Boucekkine, and J.-L. Fillaut, *Dalton Trans.*, 2013, **42**, 16773.

[S3] A. K.-W. Chan, K. M.-C. Wong, and V. W.-W. Yam, *J. Am. Chem. Soc.*, 2015, **137**, 6920.

[S4] J. Liang, Z. Chen, L. Xu, J. Wang, J. Yin, G.-A. Yu, Z.-N. Chen, and S.-H. Liu, *J. Mater. Chem. C*, 2014, **2**, 2243.

[S5] Z. Gao, Z. Li, Z. Gao, and F. Wang, *Nanoscale*, 2018, **10**, 14005.

[S6] C. Kulkarni, R. Munirathinam, and S. J. George, *Chem. Eur. J.*, 2013, **19**, 11270.

[S7] P. A. Korevaar, C. Schaefer, T. F. A. de Greef and E. W. Meijer, *J. Am. Chem. Soc.*, 2012, **134**, 13482.